Carbohydrate Polymers 97 (2013) 837–848

Contents lists available at SciVerse ScienceDirect

Carbohydrate Polymers

journal homepage: www.elsevier.com/locate/carbpol

Ternary PVA nanocomposites containing cellulose nanocrystals from different sources and silver particles: Part II

E. Fortunati[a,*], F. Luzi[a], D. Puglia[a], A. Terenzi[a], M. Vercellino[c], L. Visai[c,d], C. Santulli[e], L. Torre[a], J.M. Kenny[a,b]

[a] University of Perugia, Civil and Environmental Engineering Department, UdR INSTM, Strada di Pentima 4, 05100 Terni, Italy
[b] Instituto de Ciencia y Tecnología de Polímeros, ICTP-CSIC, Juan de la Cierva 3, 28006 Madrid, Spain
[c] Department of Molecular Medicine, UdR INSTM and Center for Tissue Engineering (C.I.T.), University of Pavia, 27100 Pavia, Italy
[d] Salvatore Maugeri Foundation IRCCS, Via S. Maugeri 4, 27100 Pavia, Italy
[e] La Sapienza University of Rome, Chemical Engineering, Materials, and Environment Department, Via Eudossiana 18, 00184 Rome, Italy

ARTICLE INFO

Article history:
Received 21 March 2013
Received in revised form 17 April 2013
Accepted 9 May 2013
Available online 16 May 2013

Keywords:
Natural fibres
Cellulose nanocrystal
Silver nanoparticles
Bio-nanocomposites
Poly(vinyl alcohol) (PVA)
Water absorption capacity

ABSTRACT

Cellulose nanocrystals (CNC) extracted from three different sources, namely flax, phormium, and commercial microcrystalline cellulose (MCC) have been used in a polyvinyl alcohol (PVA) matrix to produce anti-bacterial films using two different amounts of silver nanoparticles (0.1 wt% and 0.5 wt%). In general, CNC confer an effect of reinforcement to PVA film, the best values of stiffness being offered by composites produced using phormium fibres, whilst for strength those produced using flax are slightly superior. This was obtained without inducing any particular modification in transition temperatures and in the thermal degradation patterns. As regards antibacterial properties, systems with CNC from flax proved slightly better than those with CNC from phormium and substantially better than those including commercial MCC. Dynamic mechanical thermal analysis (DMTA) has only been performed on the ternary composite containing 0.1 wt% Ag, which yielded higher values of Young's modulus, and as a whole confirmed the above results.

1. Introduction

The use of ligno-cellulosic fibres, extracted from plants, for the reinforcement of composites, is a procedure followed in the last few years to obtain materials with an improved carbon dioxide balance. Results are promising, especially when plant fibres are coupled with a biodegradable polymer matrix, such as for example poly(lactic) acid (PLA), polyvinyl alcohol (PVA), etc., so that an improvement of mechanical properties over the pure matrix is consistently obtained using a number of fibres, either extracted from the leaves and from the bast of different plants (De Rosa et al., 2011; Fischer, Werwein, & Graupner, 2012; Shanks, Hodzic, & Ridderhof, 2006; Taha & Ziegmann, 2010; Wang, Tong, Hou, Li, & Shen, 2011). In particular, PVA is known to provide a good compatibility by penetrating vegetable tissue between the microfibrils (Hepworth & Bruce, 2000).

However, a number of limitations appear whenever cellulosic materials are intended for prospective use as a reinforcement of biodegradable polymer films, which would be in general suitable for applications e.g., in sectors, such as packaging and biomedical industry. In this case, the large dimension and considerable deviation in diameter of technical fibres discourage their application directly as film reinforcement, rather suggesting a film stacking technique for composite production (Garkhail, Heijenrath, & Peijs, 2000). Moreover, plant fibres, despite being chemically treated to assist the removal of non-structural matter, show a large presence of defects in their structure, offering eventually a mechanical performance which, albeit sufficient for most current semi-structural uses of composite panels, is very far from that of microcrystalline cellulose (Hughes, 2012). It needs to be added that some cellulosic material can be unsuitable for the production of woven tissues of areal weight compatible with their use in a composite, such as is the case for a number of leaf fibres, including phormium (Cruthers, Carr, & Laing, 2006). In other cases, it may be agro-waste or else a by-product of a crop intended for other uses, which may find another application and possibly added value by the extraction of cellulose nanocrystals (CNC) (Hassan, Mueller, Tartakowska, & Wagner, 2011).

The extraction of CNC from plant fibres is often performed through acid hydrolysis using sulphuric acid to remove the amorphous cellulose and form highly crystalline cellulose (Bondeson, Mathew, & Oksman, 2006; Siqueira, Bras, & Dufresne, 2010). CNC

* Corresponding author. Tel.: +39 0744 492921; fax: +39 0744 492950.
E-mail address: elena.fortunati@unipg.it (E. Fortunati).

0144-8617/$ – see front matter © 2013 Elsevier Ltd. All rights reserved.
http://dx.doi.org/10.1016/j.carbpol.2013.05.015

are typically a rigid rod-shaped monocrystalline cellulose domain, 1–100 nm in diameter and from tens to hundreds of nanometers in length, with morphological and structural characteristics, including entanglement and geometrical dispersion, depending on the species, cultivar and agronomical factors (e.g., plant maturity, characteristics of the soil). The yield of the extraction process (the quantity of nanocellulose obtained from a given weight of macrofibre), depends on both the crystallinity of the specific plant fibre and the procedure adopted for extraction. The method adopted in this work has been originally applied on sisal fibres by Moran, Alvarez, and Cyras, 2008 and employed already for incorporation of okra bahmia (*Abelmoschus esculentus*) fibres in a PVA matrix (Fortunati, Puglia, Monti, Santulli, Maniruzzaman, et al., 2012). The extraction method involves a first chemical treatment leading to the production of holocellulose by the gradual removal of lignin, while the subsequent sulphuric acid hydrolysis process allowed obtaining cellulose nanocrystals in an aqueous suspension.

The two lignocellulosic fibres that are considered for the extraction of CNC in this study, flax and *Phormium tenax*, the former a bast fibre, the latter a leaf fibre, have been already the object of some research work. In particular, the extraction of cellulose nanocrystals from flax (Liu, Yuan, Bhattacharyya, & Easteal, 2010) aimed at their introduction in a 160 microns solution cast PLA film resulted in a substantial improvement over the pure matrix properties. Nucleation and subsequent crystallisation of PLA was more facilitated as an effect of the presence of flax cellulose in the amorphous composites than in the crystalline ones. In the particular case of *P. tenax* leaf fibres, cellulose nanocrystals with an acicular structure ranging from 100 to 200 nm in length and 15 nm in width were extracted by acid hydrolysis (Fortunati, Puglia, Monti, Santulli, & Kenny, 2012). The specific comparison between the properties of CNC obtained from flax and from *P. tenax* has been considered elsewhere and compared with those extracted from commercial microcrystalline cellulose (Fortunati et al., 2013).

In recent years, anti-bacterial treatment of nanocellulose composites has been also considered in particular through the incorporation of heavy metals, such as ionic silver, which are recognised for their broad-spectrum biocide effects (Fortunati et al., 2011; Williams, Doherty, Vince, Grashoff, & Williams, 1989). In particular, a previous study on PLA composites based on CNC and silver particles suggested the possibility to realise multifunctional ternary composites with high performance and antimicrobial response, suitable for use as food-active packaging films (Fortunati, Armentano, Zhou, Puglia, et al., 2012).

This work is specifically aimed at comparing merits and drawbacks of three configurations of PVA composites based on CNC and silver nanoparticles, focusing on the potential of ternary systems in terms of structural, thermal and morphological properties. The effect of silver nanoparticles presence and content was deeply investigated and the combination with different kind of CNC severely discussed. The active antimicrobial properties of PVA based ternary bio-nanocomposites was studied and proved in this research.

2. Experimental part

2.1. Materials and methods

Polyvinyl alcohol (PVA) supplied by Sigma–Aldrich (M_w 124–146 kg mol^{-1}, 99% hydrolysed), is a synthetic and biodegradable polymer produced from the hydrolysis of polyvinyl acetate. The PVA was used as matrix for the nanocomposite preparation.

Microcrystalline cellulose (MCC, dimensions of 10–15 μm), supplied by Sigma–Aldrich, was used as start material in cellulose nanocrystal (CNC_MCC) synthesis and two natural fibres *P. tenax* and *Flax*, were used as raw material in the cellulose nanocrystal (CNC_ph and CNC_flax, respectively) synthesis. *P. tenax* technical fibres were obtained from New Zealand while technical *Flax* fibres were provided by Finflax Ltd.: both were supplied as long fibres.

The preparation of the cellulose nanocrystals (CNC) extracted from commercial MCC and natural *Phormium* and *Flax* fibres was described in our previous study (Fortunati et al., 2013). A two-step procedure for the extraction of nano-sized cellulose was implemented: the first chemical alkali treatment leads to the production of holocellulose by the gradual removal of lignin, while the subsequent sulphuric acid hydrolysis process allows obtaining cellulose nanocrystals in an aqueous suspension from different raw materials (Fig. 1, panel A). Transmission electron microscopy (TEM, JEOL JEM-1010) in Panel A, shows that CNC appear individualized with a similar acicular structure ranging from 100 to 250 nm in length and 15 nm in width (Fortunati et al., 2013). Commercial silver nanoparticles (Ag), purchased from PlasmaChem GmbH, Berlin, were used as antimicrobial agent in PVA matrix.

2.2. PVA/CNC/Ag nanocomposites processing

Polyvinyl alcohol (PVA) nanocomposite films reinforced with cellulose nanocrystals (CNC) and silver nanoparticles were prepared by solvent casting in water (Roohani et al., 2008). To produce the ternary film, initially the PVA pellets (2 g) were dissolved in 15 ml of distilled water at 80 °C for 2 h under mechanical stirring. Then, the obtained PVA solutions were kept under stirring to reach room temperature (RT). To obtain films with different compositions, the PVA solutions were mixed with an aqueous dispersion of different kind of cellulose nanocrystals (CNC_MCC, CNC_ph or CNC_flax) and sonicated (Vibracell 75043, 750 W, Bioblock Scientific) for 2 min. Cellulose nanocrystals were added at 1 wt% respect to the PVA matrix, on the base of our previous results (Fortunati et al., 2013). At the same time the hydrophilic silver nanoparticles were dissolved in 10 ml of distilled water and placed in a sonication bath for 2 h at room temperature. The Ag aqueous solution thus obtained was mixed under mechanical stirring with the dissolved polymer solution containing 1 wt% of CNC for 2 h at 25 °C. The resulting mixture was cast in Teflon® and placed in an oven at 37 °C to evaporate water. Silver nanoparticle contents in the final bionanocomposites were 0.1 wt% and 0.5 wt% respect to the polymer weight and the obtained films were 200–300 μm thick.

Ternary bio-nanocomposite films containing 1 wt% of CNC_MCC, CNC_ph or CNC_flax respect to the PVA polymer matrix, and 0.1 wt% or 0.5 wt% of silver nanoparticles (Ag), were obtained. Resulting samples were designated as PVA, PVA/1CNC_MCC/0.1 Ag or PVA/1CNC_MCC/0.5 Ag, PVA/1CNC_ph/0.1 Ag or PVA/1CNC_ph/0.5 Ag, and PVA/1CNC_flax/0.1 Ag or PVA/1CNC_flax/0.5 Ag, respectively.

2.3. Characterization methods

2.3.1. Silver nanoparticle characterization

The morphology of silver nanoparticles was examined by field emission scanning electron microscopy (FESEM, Supra 25-Zeiss, Germany). Ag nanoparticles were suspended in distilled water by ultrasound (Ultrasonic bath-mod.AC-5, EMMEGI, Italy) for 2 h and few drops of the suspension were deposited onto a substrate of silicon, dried at room temperature and visualized.

Silver nanoparticles absorption spectra were recorded by a UV–vis spectrophotometer (Perkin Elmer Instruments (Lambda 35)), working in the wavelength between 250 and 900 nm. Few

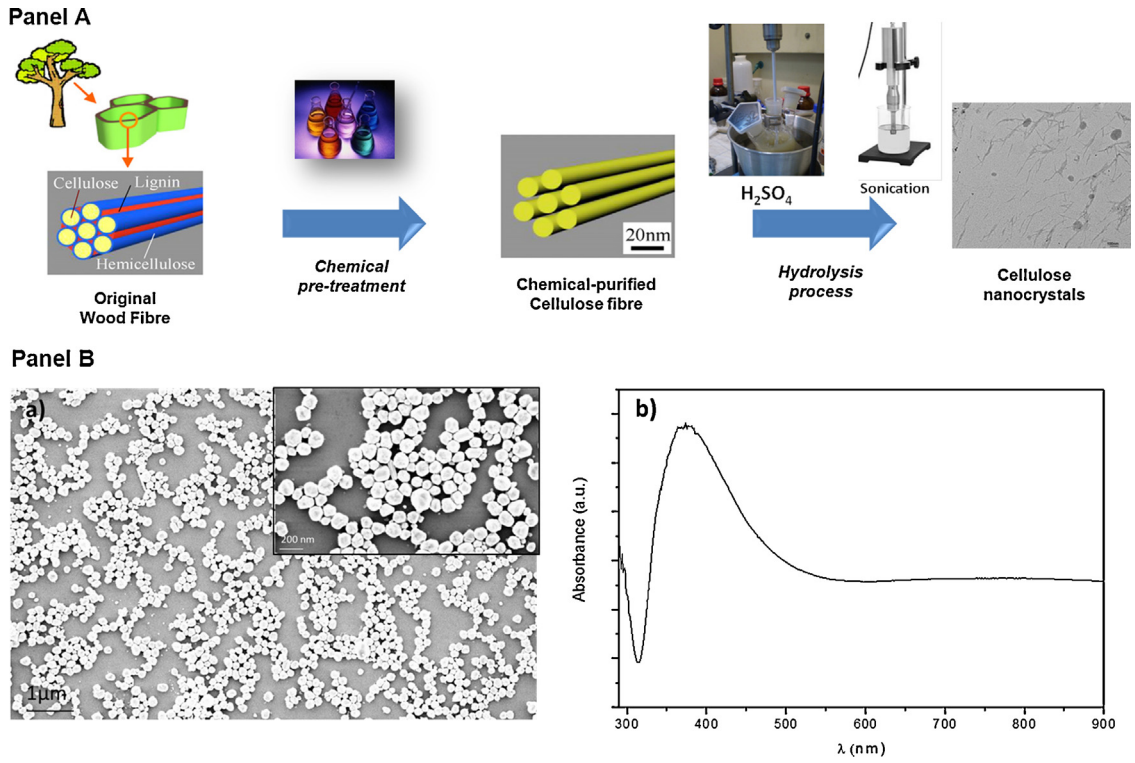

Fig. 1. Panel A: Scheme of CNC extraction process. Panel B: FESEM investigation (a) and UV–vis absorption spectrum (b) of silver nanoparticles.

drops of the Ag suspension were deposited on a glass substrate, dried at room temperature and analyzed.

2.3.2. PVA nanocomposite characterization

Differential scanning calorimeter (TA Instrument, Q200) measurements were performed in the temperature range from −25 to 240 °C, at 10 °C/min, performing two heating and one cooling scan. The glass transition temperature (T_g) was taken as the inflection point of the specific heat increment at the glass–rubber transition while the melting temperature (T_m) and the crystallization temperature (T_c) was taken as the peak temperature of the endotherm and exothermic, respectively. Three samples were used to characterize each material.

The cristallinity degree was calculated as:

$$\chi = \frac{1}{1 - m_f}\left[\frac{\Delta H}{\Delta H_0}\right] \times 100 \quad (1)$$

where ΔH is the enthalpy for melting or crystallization, ΔH_0 is enthalpy of melting for a 100% crystalline PVA sample, taken as 161.6 J/g (Roohani et al., 2008) and $(1-m_f)$ is the weight fraction of PVA in the sample. Three samples were tested for each formulation and data expressed as their average ± standard deviation.

Thermogravimetric measurements (TGA) were performed by using a Seiko Exstar 6300. Heating scans from 30 to 600 °C at 10 °C/min in nitrogen atmosphere were performed for each sample. Three samples were tested for each formulation and data expressed as their average ± standard deviation.

The microstructure of PVA nanocomposite films was investigated by scanning electron microscope, FESEM, Supra 25-Zeiss. For fracture analysis, brittleness was enhanced using liquid nitrogen, then the fracture sections of the nanocomposites were analysed following gold sputtering of the samples. Neat PVA and the nanocomposites were analysed in transparency performing absorption measurements by means UV–vis spectrophotometer (Perkin Elmer Instruments (Lambda 35)), working in the wavelength between 250 and 900 nm, to investigate the optical properties of the produced composites.

Structural analysis was performed by using the Fourier infrared (FT-IR, Jasco FT-IR 615 spectrometer in the 400–4000 cm^{-1} range) spectra of neat PVA and PVA nanocomposites. For the measurement few drops of PVA/CNC/Ag solution were cast on silicon wafer for each formulation and investigated in transmission mode.

The characterization of mechanical behaviour of neat PVA and PVA/1CNC/Ag was carried out by performing tensile tests and dynamic mechanical analysis in temperature. The tensile tests were carried out on preformed rectangular specimens (100 mm × 10 mm) on the basis of UNE-EN ISO 527-5 with a crosshead speed of 5 mm/min, a load cell of 500 N and an initial gauge length of 50 mm. The specimens were dried in a vacuum oven at 40 °C for 72 h, and then cooled in a desiccator and immediately tested, in view of the high capability of PVA to absorb water. The measurements were done at room temperature. The stress–strain curves allowed measuring average tensile strength (σ_b), elongation at break (ε_b), while Young's modulus (E) was calculated from the resulting stress–strain curves. Five samples were tested for each formulation and data expressed as mean ± standard deviation. Dynamic mechanical thermal analysis (DMTA) tests were also done on preformed rectangular specimens (100 mm × 10 mm) on the basis of procedures reported in the ASTM D 4065 standard. The measurements were conducted by setting the following parameters: frequency 1 Hz, deformation 0.3%, initial temperature −20 °C, final temperature 100 °C, ramp rate 3 °C/min. Five samples were tested for each formulation and data expressed as mean ± standard deviation.

2.3.3. Water absorption test of PVA bio-nanocomposites

The water absorption capacity of the nanocomposite films was measured on plastic sheets of 10 mm × 20 mm. The specimens were

first dried in a vacuum oven at 40 °C for 72 h, then cooled in a desiccator and immediately weighed. The conditioned specimens were fully immersed in a container filled with distilled water. The test was conducted 4 °C, at 24 °C and 37 °C in triplicate for all formulations and each specimen was taken off from the container, the surface water was removed by adsorbing it using filter paper, and then weighed. The result of each sample represents the average of three tests. The water absorption capacity (WAC) was calculated as:

$$\mathrm{WAC\%} = \frac{W_A - W_I}{W_I} \times 100 \quad (2)$$

where W_A is the weight of the specimen at the adsorbing equilibrium and W_I is the initial dry weight of the specimen. Visual observation of the samples at different incubation times was also performed in order to evaluate the effect of water absorption on the dimension and shape of the specimens.

2.3.4. Antibacterial activity

The microorganisms used in this study were *Escherichia coli* RB (*E. coli* RB) and *Staphylococcus aureus* 8325-4 (*S. aureus* 8325-4). *E. coli* RB was an isolate provided by the "Zooprofilattico Institute of Pavia", Italy, whereas *S. aureus* 8325-4 was a gift from Timothy J. Foster (Department of Microbiology, Dublin, Ireland). *E. coli* RB was routinely grown in Luria Bertani Broth (LB) (Difco, Detroit, MI, USA) and *S. aureus* 8325-4 in Brian Heart Infusion (BHI) (Difco) overnight under aerobic conditions at 37 °C using a shaker incubator (New Brunswick Scientific Co., Edison, NJ, USA). These cultures, used as source for the experiments, were reduced at a final density of 1×10^{10} cells/ml as determined by comparing the OD_{600} of the sample with a standard curve relating OD_{600} to cell number.

To evaluate the antimicrobial activity of PVA and PVA bio-nanocomposites films, 100 μl (1×10^4) of an overnight diluted cell suspension of *E. coli* RB or *S. aureus* 8325-4 was added to each sample seeded at the bottom of 96-well tissue culture plate and incubated at different temperatures (37 °C, 24 °C and 4 °C) for 3 h and 24 h, respectively. In this way, the effect of temperature on the antibacterial activity efficiency exerted by PVA and PVA bio-nanocomposites as food packaging was investigated. It is a common practice to store food at 4 °C in refrigerators, but it is also likely that under transportation food undergoes higher temperature of storage (24 °C and/or 37 °C). Furthermore, 96-well flat-bottom sterile polystyrene culture plates (TCP) used as controls were incubated for the same temperatures and times. At the end of each incubation time, the bacterial suspension was then serially diluted, and plated on the LB (*E. coli*) or BHI (*S. aureus*) agar plates, respectively. The plates were then incubated for 24 h/48 h at 37 °C. Cell survival was expressed as percentage of the CFU (Colony-Forming Unit) of bacteria grown on PVA and PVA-bionanocomposite films to CFU of bacteria grown on 96-well TCP.

2.3.5. Statistical analysis

S. aureus and *E. coli* cells grown on 96-well TCP were used as positive controls. The bacterial viability in positive control experiments was used as the reference (100%). The surviving fractions, expressed as percentage, of both bacterial strains on PVA and PVA-bionanocomposite films were compared with the positive control. All data are expressed as the mean and SD. Differences in the study variables according to different experimental conditions were calculated using one-way analysis of variance (ANOVA), followed by Bonferroni's post hoc test. A two-tailed p value < 0.05 was considered statistically significant. All calculations were generated using GraphPad Prism 5.0 (GraphPad Inc., San Diego, CA).

3. Results and discussion

3.1. Silver nanoparticle morphology and absorbance study

The morphological characterization of silver nanoparticle (Ag) was shown in Fig. 1 (panels B and a) at two different magnifications. FESEM micrograph shows that the Ag particles have a diameter distribution ranging from 100 nm to 150 nm and showed a spherical like-shape.

Fig. 1 (panels B and b) shows UV–vis absorption spectrum of silver nanoparticles. The absorption spectrum of silver nanoparticles presents a main broad band with a maximum at 375 nm due to the surface plasmon resonance of silver nanoparticles (Lok et al., 2007). This justifies the yellow color of the aqueous solution during the solvent casting process and the final appearance of PVA bio-nanocomposites.

3.2. Thermal analysis of PVA and PVA bio-nanocomposites

The thermal analysis was used to highlight the modification of PVA and its nanocomposites in different temperature ranges. More in detail, differential scanning calorimetry (DSC) was used to study the glass transition, crystallization and melting phenomena of PVA and PVA nanocomposites in relation to their preparation method and their composition: DSC thermal properties are summarized in Table 1. DSC analysis allowed determining the effects of the inclusion of different types of CNC and silver nanoparticles in a matrix of pure PVA. The PVA heating thermograms displayed both the glass transition temperature (T_g) and the melting endotherm at T_m. PVA film exhibited a relatively large and sharp endothermic curve with a peak at around 217 °C, while at around 73 °C there is an increment of heat corresponding to the glass transition temperature of the polymer. In PVA film, an exothermic crystallization is apparent during the cooling scan at around 189 °C (Fortunati et al., 2013). The nanocomposites reinforced with different kinds of CNC and two different content of silver nanoparticles examined with DSC exhibit the same trend of pure PVA. The nanocomposites studied do not change significantly their glass transition temperature respect to pure PVA used as matrix. This result is in accordance with the studies reported in literature also for binary systems reinforced only with cellulose nanocrystals, which do not indicate a large variation of glass transition temperature (Fortunati, Puglia, Monti, Santulli, Maniruzzaman, et al., 2012; Fortunati et al., 2013) and also with the results on ternary systems obtained elsewhere in literature (George, Vallayil, Ramana, Shanmugam, & Siddaramaiah, 2012; Mahanta & Valiyaveettil, 2012; Vivekanandhan, Christensen, Misra, & Mohanty, 2012). The T_g of polymer nanocomposites can be affected by the level of interaction between polymer chains and the reinforcing nanoparticle. Here the T_g was found to be decreasing with the addition of silver nanoparticles, which suggests that the addition of Ag nanoparticles led to a decrease in the interaction between polymer chains and an increase in free volume inside the lattice. The combination of CNC and silver nanoparticles in a PVA matrix led also to an increase in the degree of crystallization measured during the cooling scans. Moreover, ternary systems showed also a crystallization temperature (T_c) higher by about 10 °C respect to neat PVA (T_c = 188.9 ± 0.2 °C). This result clearly evidences that CNC are able to promote the crystallization of the PVA matrix, acting as heterogeneous nucleating agents. It can be also observed that an increase in the Ag content does not affect crystallinity of the neat PVA (melting enthalpies in Table 1 are almost unchanged), while lower degrees of crystallinity for ternary systems with respect of binary systems containing equivalent content (1 wt%) of CNC obtained from MCC and flax (Fortunati et al., 2013) were detected after the second heating scan. A nucleating effect was indeed observed in the case of PVA/CNC_ph (X_m values of 19.8 ± 0.7

Table 1
Results from DSC and TGA tests of PVA and PVA bio-nanocomposite films.

Samples	Cooling scan				Second heating Scan				TGA		
	T_g (°C)	ΔH_c (J/g)	T_c (°C)	X_c	T_g (°C)	ΔH_m (J/g)	T_m (°C)	X_m	$T_{second\ peak}$ (°C)	$T_{third\ peak}$ (°C)	Residual mass (%) at 600 °C
PVA	73.1 ± 0.1	48.5 ± 2.1	188.9 ± 0.2	30.0 ± 1.3	76.6 ± 0.9	38.1 ± 3.9	217.3 ± 0.1	23.5 ± 2.4	267.0 ± 2.0	430.0 ± 2.9	10.0 ± 1.0
PVA/1CNC_MCC/0.1 Ag	70.5 ± 1.4	51.2 ± 5.4	196.2 ± 0.5	32.1 ± 3.4	76.5 ± 0.4	39.4 ± 1.1	221.6 ± 0.1	24.7 ± 0.7	261.2 ± 1.1	431.2 ± 2.1	10.8 ± 1.0
PVA/1CNC_MCC/0.5 Ag	71.8 ± 2.3	51.6 ± 3.2	194.2 ± 1.3	31.7 ± 2.0	77.5 ± 0.2	41.8 ± 1.6	219.7 ± 0.9	26.2 ± 1.0	260.4 ± 2.1	429.3 ± 2.3	11.2 ± 0.4
PVA/1CNC_ph/0.1 Ag	73.5 ± 4.0	50.2 ± 4.1	195.2 ± 1.9	31.4 ± 2.5	77.8 ± 2.8	45.2 ± 2.2	219.1 ± 1.8	28.3 ± 1.4	257.6 ± 2.3	427.9 ± 3.0	10.9 ± 1.2
PVA/1CNC_ph/0.5 Ag	71.4 ± 1.2	54.9 ± 1.0	195.9 ± 2.3	30.5 ± 0.7	76.5 ± 0.2	38.9 ± 0.3	219.8 ± 1.5	20.5 ± 0.2	257.8 ± 1.2	430.1 ± 3.1	11.4 ± 0.5
PVA/1CNC_flax/0.1 Ag	71.6 ± 0.5	48.5 ± 2.8	198.0 ± 1.6	30.4 ± 1.7	76.9 ± 0.2	34.4 ± 0.2	218.7 ± 0.2	21.6 ± 0.1	261.1 ± 2.0	432.2 ± 3.2	10.6 ± 1.0
PVA/1CNC_flax/0.5 Ag	72.1 ± 0.6	47.7 ± 2.6	194.6 ± 0.2	30.6 ± 1.7	80.0 ± 1.8	38.0 ± 1.7	220.9 ± 0.2	23.8 ± 1.1	262.4 ± 2.3	429.1 ± 2.1	11.6 ± 0.6

for PVA/1CNC_ph and 28.3 ± 1.4 for PVA/1CNC_ph/0.1 Ag). The shift of the melting peak to higher temperatures with an increase in the inorganic phase content was also observed, which can be explained by the reduced mobility of the PVA chains attached to the surface of the Ag nanoparticles. This is likely to suggest that the purpose of broadening the temperature range for the service and workability of the PVA matrix has been reached.

The nanocomposites were also evaluated by thermogravimetric analysis in nitrogen atmosphere, in order to put in evidence the degradation behaviour and the effect of silver presence and content on their thermal stability. In Table 1 the peak temperatures for the main degradation steps of PVA pure film and PVA nanocomposites, are reported. All the investigated samples showed a similar degradation trend with a multi-step degradation. The initial weight loss (first peak) centred at around 130 °C can be attributed to the loss of moisture after initial heating. The second and third degradation steps, that were present for all studied formulations, were consistent with the generally accepted degradation mechanism of PVA (dehydration of the PVA polymer followed by chain scission and decomposition) (Frone et al., 2011; Li, Yue, & Liu, 2012). The second peak temperature related to the decomposition of pure PVA was similar for all the PVA/CNC/Ag nanocomposites, with an observed decrease (5–10 °C) of $T_{second\ peak}$ with the presence of silver nanoparticles. This behaviour was also observed in a similar system (PLA based films loaded with nanocrystals extracted from MCC) containing silver nanoparticles and it was due to the presence of thermally conductive Ag particles (Fortunati, Armentano, Iannoni, & Kenny, 2010). However, a slight increase of $T_{second\ peak}$ temperature was detected for ternary systems based on CNC_MCC or CNC_ph if compared with the respective binary formulations, objectives of our previous work (Fortunati et al., 2013). The observed small improvement in the thermal stability of the ternary systems can be explained through the reduced mobility of the PVA chains in the nanocomposite induced by the combined presence of silver nanoparticles and cellulose structures. This behaviour is also a consequence of the attachment of the PVA chains to the surface of the Ag particles (further confirmed by FTIR measurements). Only in the case of PVA/1CNC_flax/0.1 Ag and PVA/1CNC_flax/0.5 Ag, when compared with PVA/1CNC_flax corresponding binary system, a decrease of $T_{second\ peak}$ was detected. Indeed, weighing the char residue at the end of the tests, higher residual masses in the systems having the higher percentage of silver nanoparticles were observed, as expected.

3.3. Morphological and transparency properties of PVA bio-nanocomposites

Field emission scanning electron microscopy of neat PVA and PVA bio-nanocomposite fracture surfaces were investigated in order to evaluate the samples morphology and to analyse the dispersion of cellulose nanocrystals and silver nanoparticles inside the polymer matrix (Fig. 2). FESEM images show a smooth and uniform PVA fracture surface (Fig. 2a and b), while an increased texture roughness was observed with the presence of cellulose nanocrystals combined with silver nanoparticles. The fractured surface of bio-nanocomposites appears to be rougher respect to the PVA film, as just reported for PVA/CNC binary systems (Fortunati et al., 2013). The cellulose nanocrystals have a clear tendency to aggregate due to their strong hydrogen bonding property, which leads to the formation of a percolating network that is responsible of increased roughness, but also of the enhanced mechanical response of bio-nanocomposite films. Moreover, FESEM analysis highlights the presence of some white spots, which can be attributed to the silver nanoparticles that appear well distributed through the surface. However, it was very difficult to identify the crystal structure and the distribution of silver nanoparticles inside the PVA, due to

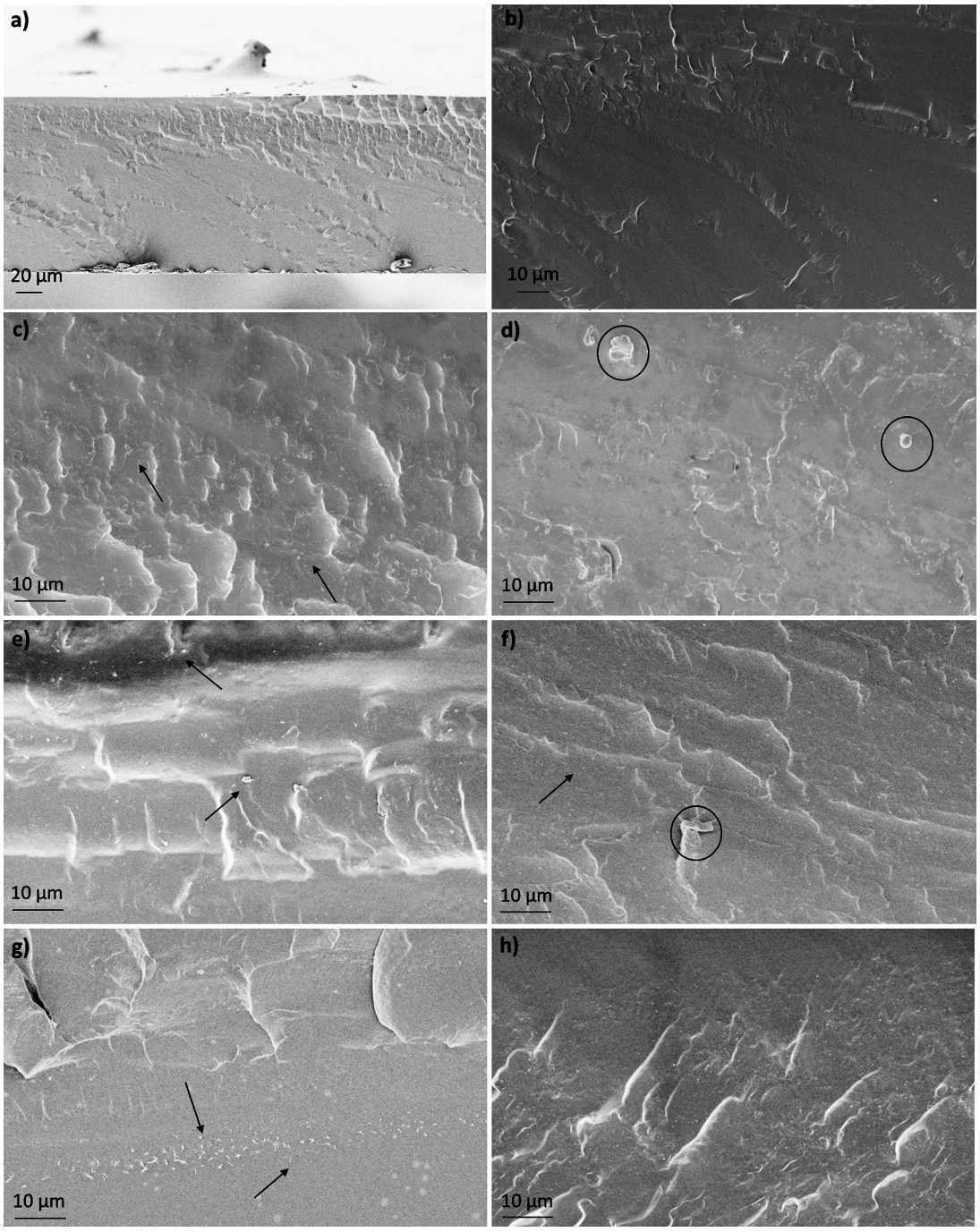

Fig. 2. Morphological investigation of PVA and PVA ternary bio-nanocomposite fractured surface.

the low contrast between PVA and cellulose and to the nano-scale of the reinforcing phases (Bondeson, Syre, & Oksman, 2007). For this reason, visual observation and UV–vis absorption measurements were carried out in order to obtain more information about the distribution of the cellulose and the silver inside the polymer matrix.

The results from the absorption UV–vis measurements and the visual observations, shown in Fig. 3, confirm the efficiency of the processing procedure of PVA bio-nanocomposites. PVA is a transparent polymer (transmittance of 93% at 700 nm wavelength), well known for its film forming properties. The transparency of PVA matrix is maintained for the bio-nanocomposite ternary films reinforced with 1 wt% of cellulose nanostructures and 0.1 wt% of Ag. A percentage of transmitted light between 55 and 65% (Fig. 3, panel B) was maintained for PVA/CNC/0.1 Ag different systems, as confirmed also by visual observation (Fig. 3, panel C). A different behaviour was detected for PVA bio-nanocomposites loaded with the higher content of silver nanoparticles (0.5 wt%) confirmed both by the qualitative analysis (Fig. 3, panels A and C) that by the quantitative analysis (Fig. 3, panel B). The systems reinforced with the 0.5 wt% of silver nanoparticles have, in fact, a transmittance of 36–38% at 700 nm, while the formation of a peak centred at around 450 nm and a less intense peak at 375 nm attributed to the Ag surface plasmon resonance, was detected for ternary PVA bio-nanocomposites. The transparent nature of PVA is affected by the addition of Ag and this effect is more evident with the higher amount of silver nanoparticles, so that it was found that high transparency levels were maintained when CNC are combined with only 0.1 wt%

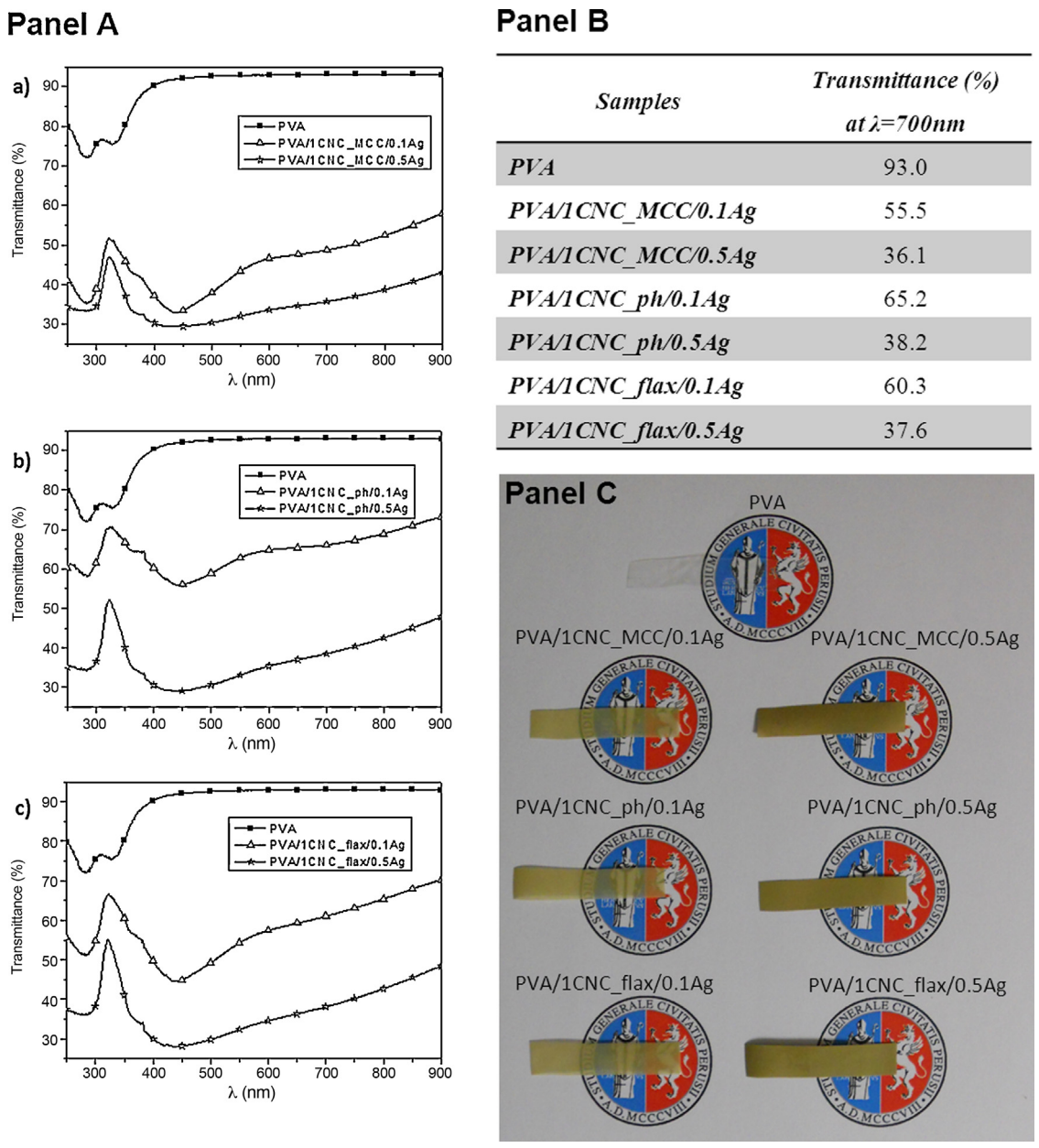

Fig. 3. UV–vis analysis (panel A), trasmittance values at 700 nm (panel B) and visual observation of the solvent casting of PVA and PVA ternary bio-nanocomposites.

of silver nanoparticles. On the other side, low levels of transmission in the UV range can make PVA based ternary nanocomposites an excellent barrier to prevent UV light-induced lipid oxidation when applied in food systems. Visual observation (Fig. 3, panel C) shows that no agglomeration effects were revealed, confirming the good dispersion of CNC and silver nanoparticles obtained during the processing of PVA bio-nanocomposites.

3.4. Mechanical behaviour of PVA bio-nanocomposites

Tensile test and dynamic mechanical thermal analysis were performed in order to evaluate the effect of CNC type and their combination with silver nanoparticles on the elastic and plastic response of the bio-nanocomposites.

The results of tensile tests are reported in Table 2. By observing the data it is possible to note that all the produced bio-nanocomposites have significantly higher modulus and strength when compared with pure PVA film. These effects are achieved by maintaining a ductile behaviour in bio-nanocomposites, with minor or in some case negligible influence on failure strain (Table 2), as indicated by the stress–strain curves in Fig. 4a. These results outline the efficiency of the combination of cellulose with low contents of Ag in strengthening the PVA matrix. It is also interesting to analyse the effect of Ag nanoparticles on the mechanical

Table 2
Results from tensile test of PVA and PVA bio-nanocomposite films.

Samples	Tensile test		
	σ_b (MPa)	ε_b (%)	E_{young} (MPa)
PVA	25 ± 4	250 ± 10	210 ± 15
PVA/1CNC_MCC/0.1 Ag	46 ± 1	225 ± 10	745 ± 40
PVA/1CNC_MCC/0.5 Ag	47 ± 3	240 ± 15	550 ± 25
PVA/1CNC_ph/0.1 Ag	48 ± 3	210 ± 20	775 ± 40
PVA/1CNC_ph/0.5 Ag	43 ± 2	200 ± 20	625 ± 40
PVA/1CNC_flax/0.1 Ag	45 ± 2	225 ± 4	785 ± 50
PVA/1CNC_flax/0.5 Ag	49 ± 1	265 ± 10	560 ± 15

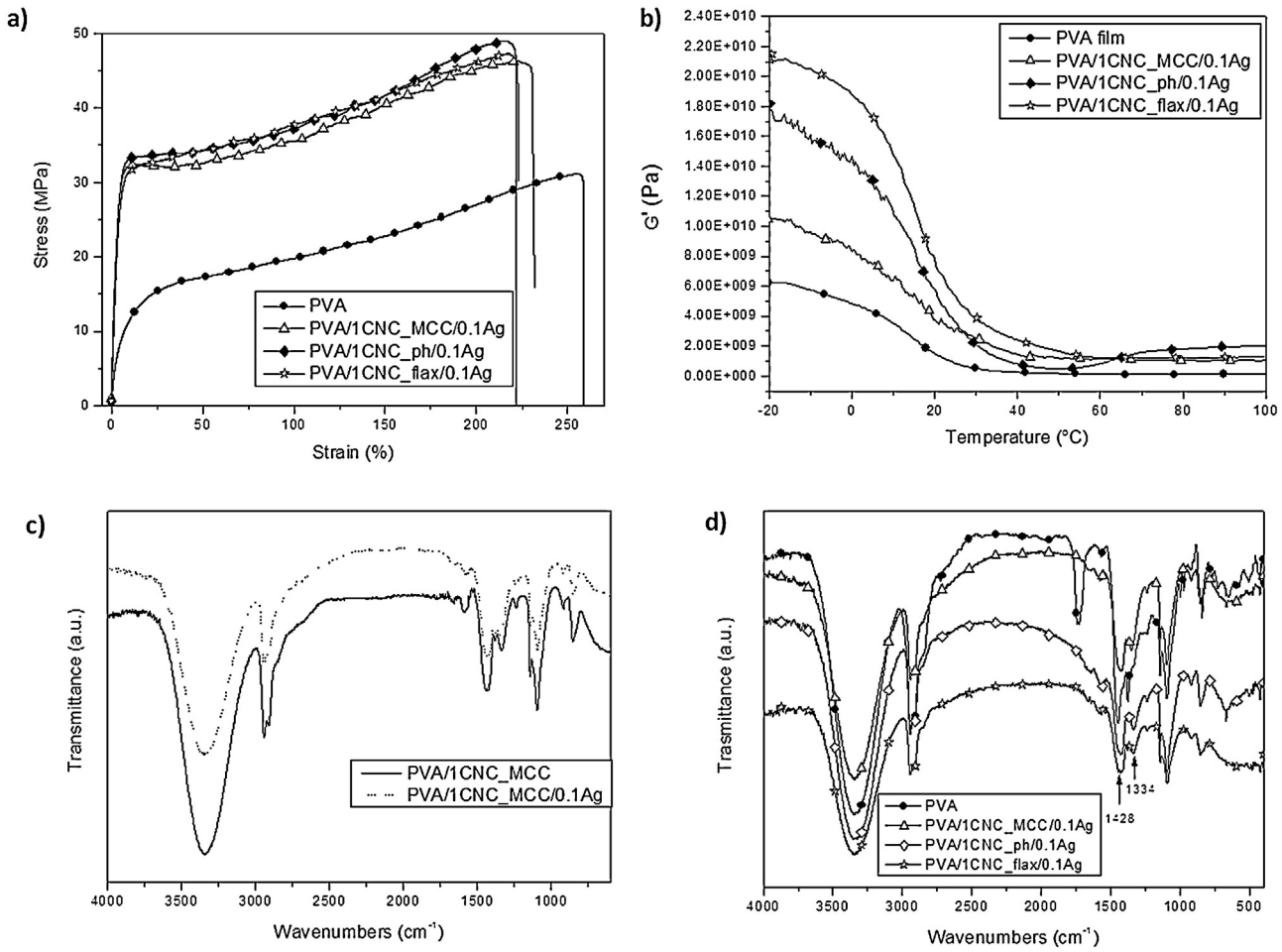

Fig. 4. Tensile test curves (a), DMTA analysis (b) and FT-IR spectra (c) and (d) of PVA and PVA ternary bio-nanocomposites.

behaviour of PVA. If the binary systems with only CNC are taken into consideration (Fortunati et al., 2013), it is possible to assert that Ag nanoparticles give an extremely high contribution on mechanical performance of bio-nanocomposites. In fact, the presence of 0.1 wt% of Ag nanoparticles determines an improvement of strength of around 20% for PVA/1CNC_MCC and PVA/1CNC_flax bio-nanocomposites and around 50% for PVA/1CNC_ph film. The effects on modulus are significantly higher with improvements higher than 150% for all binary systems with the presence of 0.1 wt% of Ag nanoparticles. Moreover ternary systems maintain a ductile behaviour and the effect of Ag nanoparticles on failure strain is in general low if binary systems are taken as reference. However, increasing the Ag nanoparticle content does not have a positive effect on the mechanical behaviour of nanocomposites. In fact, the systems with 0.5 wt% of Ag show higher strength and modulus than the pure matrix, but have low strength and modulus if compared to systems with 0.1 wt% of Ag nanoparticles. This effect of Ag nanoparticles has been observed by other authors both in PVA systems and in other polymeric systems. This behaviour suggests that the intercross-linking of PVA chain due to the presence of hydrogen bonding is affected by the presence of Ag nanoparticles (Chou, Hsu, Chang, Tseng, & Lin, 2006; Fortunati, Armentano, Zhou, Iannoni, et al., 2012; Gautam & Ram, 2010).

DMTA analysis has been performed on the systems containing only 0.1 wt% of Ag nanoparticles, since they offered the best mechanical performance. The results in terms of storage modulus (G') are reported in Fig. 4b. These are in line with Young's modulus values observed in tensile conditions: in particular, at room temperature the highest storage modulus is shown by CNC_flax and the lowest is given by CNC_MCC. By observing the behaviour of CNC_ph based formulation, it can be also noted that higher values of G' are measured for temperatures exceeding 55 °C. This increase in storage modulus has been explained by the presence of some solvent entrapped into the formulation that evaporates around that temperature.

No particular influence of the different formulations on glass transition temperature has been observed in DMTA test, thus confirming the results of DSC experiments.

3.5. Structural analysis of PVA and PVA bio-nanocomposites

The chemical structure of pure PVA and PVA ternary systems was investigated by means of FT-IR analysis and the results are reported in Fig. 4c and d. The spectrum of pure PVA shows several peaks characteristic of stretching and bending vibrations of —OH, —CH, C=C and C—O groups. The presence of cellulose nanocrystals in PVA matrix leads to the variation on the intensity of —OH stretching (centred at 3341 cm^{-1} for neat PVA). This slight variation can be attributable to the interaction between —OH group on the surface of CNC and the —OH group in the PVA matrix. As already observed (Fortunati et al., 2013), the addition of CNC has resulted in the appearance of two additional peaks in the spectra. The band at 1165 cm^{-1} corresponds to the asymmetric ring breathing mode of cellulose while the band at 1050 cm^{-1} corresponds to the C—OH bending vibrations of alcohol groups present in cellulose. Compared with the PVA binary films (PVA/1CNC_MCC), the FTIR spectra of ternary system (PVA/1CNC_MCC/0.1 Ag) shows an increase in the absorbance of the band at 1334 cm^{-1}, in comparison

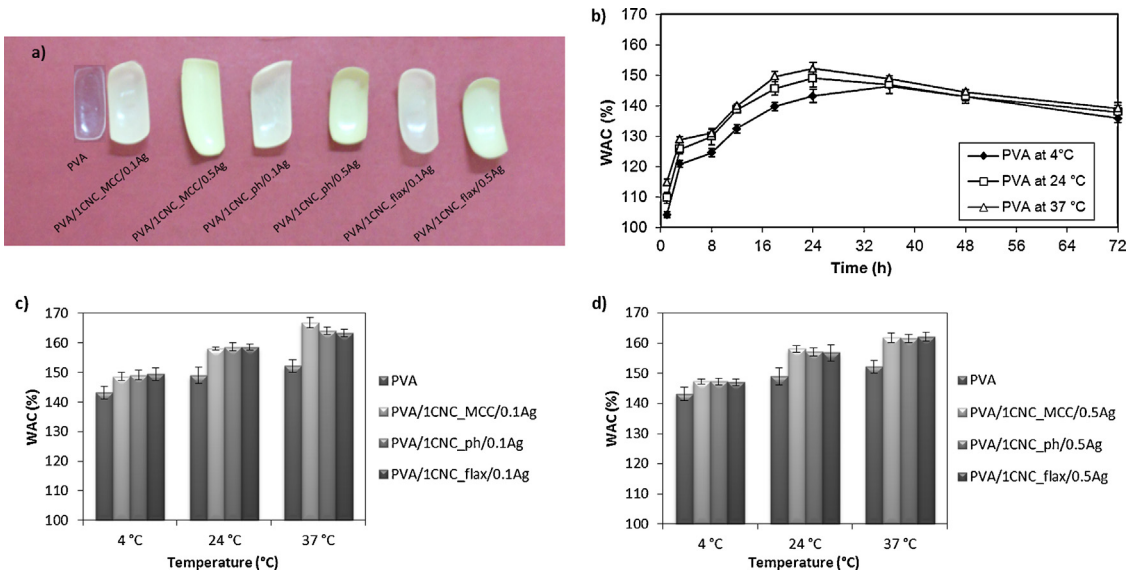

Fig. 5. Visual appearance of PVA and PVA ternary bio-nanocomposites after water absorption analysis (a), PVA water absorption capacity kinetic (b) and WAC values at different test temperatures for PVA ternary bio-nanocomposites loaded with lower (0.1 wt%) and higher (0.5 wt%) content of silver (c and d respectively).

with the band at 1428 cm^{-1} (Fig. 4c). In alcohols, the band at 1334 cm^{-1} is the result of the coupling of the O—H in-plane vibrations (strong line at 1420 cm^{-1}) with the C—H wagging vibration. Therefore, the decreased ratio between the intensities of this band and the band at 1428 cm^{-1} with the presence of 0.1 wt% of Ag nanoparticles indicates interaction between the Ag nanoparticles and the O—H groups originating from the PVA chains (Fig. 4d). Moreover, the band at 1428 cm^{-1} is shifted towards low frequency region when the silver content increases (data not shown) (Mbhele et al., 2003). These observations support a modification of the O—H interactions in the ternary systems in comparison with the neat PVA film, confirming that interactions are also established between the polymer O—H groups and the silver nanoparticles.

3.6. Water absorption

The water absorption capacity of PVA and PVA ternary bio-nanocomposites was investigated in deionised water at 4, 24 and 37 °C. The kinetics of water diffusion through the PVA and ternary films and the effect on water absorption of the type and amount of cellulose nanocrystals combined with the effect of silver presence and amount was measured by following the weight gain of the films with time (Fig. 5). Water absorption in the film is rapid at short times (<24 h), and all the tested materials loaded with different kind of cellulose and amount of silver nanoparticles reached the saturation limit after 24 h (Fig. 5). A barrier effect of silver nanoparticles, able to decrease the water absorption capacity, was revealed, since low values of WAC were detected for nanocomposites loaded with the higher amount of Ag (0.5 wt%). Moreover, WAC values at the saturation limit measured for these ternary systems were lower than those of the respective binary nanocomposites studied elsewhere (Fortunati et al., 2013). It is well known that the diffusion and transport properties through polymer films are influenced by different factors such as the tortuosity of their path through the polymer structure, the degree of exfoliation or dispersion, the filler content and orientation, the filler-induced crystallinity, the polymer chain immobilization and the filler-induced solvent retention and porosity (Sanchez-Garcia, Gimenez, & Lagaron, 2008). The presence of Ag increases the path tortuosity of the films reducing their diffusion capability respect to the binary systems.

Finally, it can be noticed that the test temperature strongly affects the WAC values for all the studied films. Lower WAC values were measured for the materials tested at 4 °C, while the higher water absorption capability was detected for all systems at 37 °C. The test temperature influenced the diffusion mechanism and the swelling properties of the PVA matrix favouring the diffusion mechanism through the polymer matrix. This phenomenon can justify the following results about the antibacterial response of different systems, studied always at 4, 24 and 37 °C.

3.7. Antibacterial properties

Fig. 6 shows the viability of *S. aureus* (panels A and B) and *E. coli* (panels C and D) cells onto PVA and PVA bio-nanocomposite films after 3 h and 24 h incubation at 4 °C, 24 °C and 37 °C, respectively. A difference in viability for both bacterial strains between PVA and PVA-bio-nanocomposite films was observed for each incubation time and temperatures. As expected, PVA and PVA/CNC binary systems (loaded with CNC_MCC, CNC_ph or CNC_flax) without Ag nanoparticles did not show any significant antibacterial activity at the incubation times and tested temperatures ($p > 0.05$). PVA/CNC/Ag films enriched with different concentrations of Ag nanoparticles (0.1 wt% or 0.5 wt%) showed an Ag dose-dependent antibacterial activity against *S. aureus* (Fig. 6, panels A and B) and *E. coli* (Fig. 6, panels C and D) strains but with some differences. The antibacterial activity was greater on *E. coli* than on *S. aureus* cells regardless of the times and temperatures of incubation. These results are in agreement with previous studies indicating that Ag nanoparticles are more toxic to *E. coli* than to *S. aureus* (Li et al., 2010; Wen-Ru et al., 2011). Nevertheless, in our experimental conditions, it is plausible to suggest that bacteria killing is not due to direct cells interaction with the Ag nanoparticles, since these are in the range of 100–150 nm, but most likely to Ag^+ ions release. Recent studies showed that Ag nanoparticles in the range of 10–20 nm can more easily disrupt the membranes of bacteria, therefore getting to their nuclear matter (Bin Ahmad et al., 2012). The reduced antibacterial activity on PVA bio-nanocomposites for *S. aureus* may be due to the structural difference in the cell wall of Gram-positive if compared to Gram-negative cells. In fact, the greater thickness of the peptidoglycan layer in the cell walls of Gram-positive cells when compared to Gram-negative ones may protect the former cells from

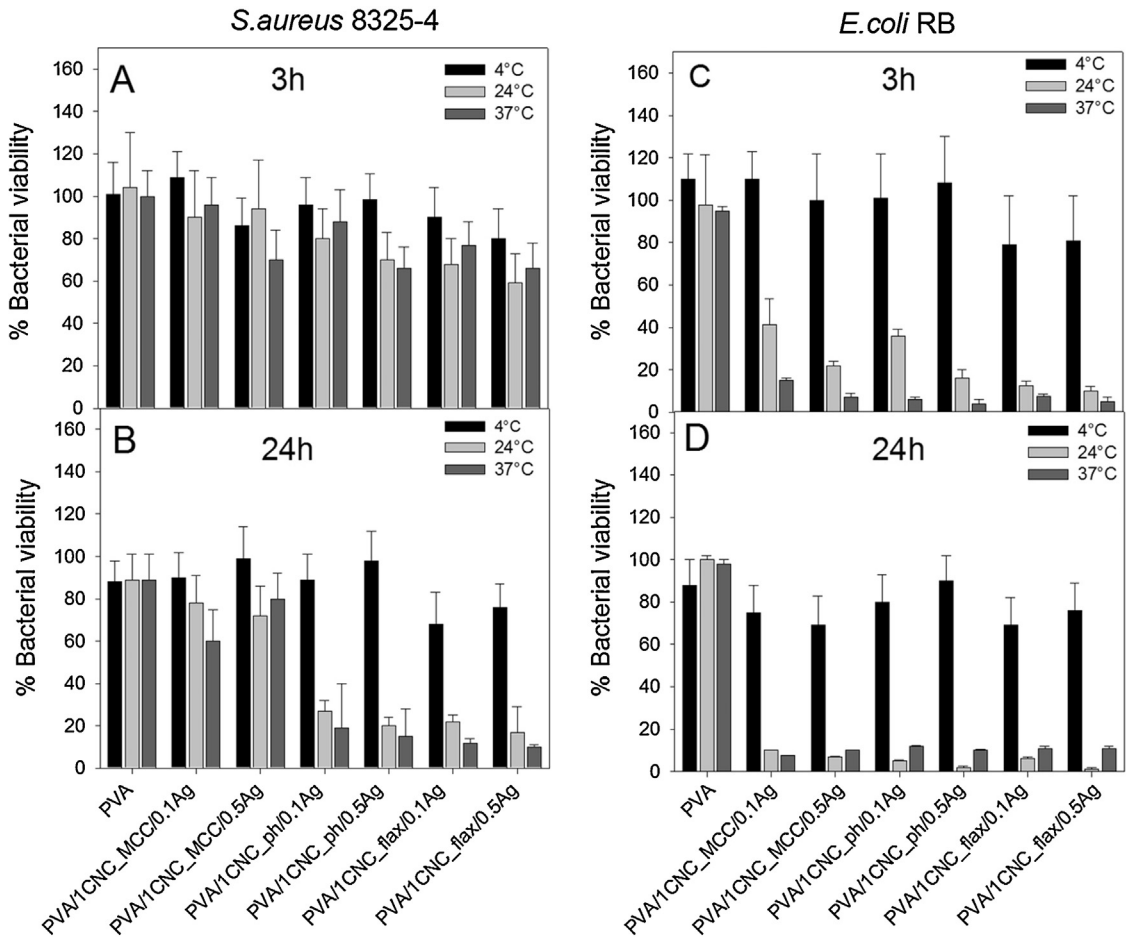

Fig. 6. Antibacterial properties of PVA and PVA-bionanocomposites at different incubation times and temperatures. *S. aureus* 8325-4 (A, B) and (C, D) cells were incubated on PVA and PVA-bionanocomposites films for 3 h (A, C) and 24 h (B, D) at 4 °C, 22 °C and 37 °C as reported in Materials and Methods Section. Results are expressed as percentage of the CFU of bacteria grown on PVA and PVA-bionanocomposites to CFU of bacteria grown on 96-well TCP and are presented as an average value ± standard deviation.

the penetration of silver ions into the cytoplasm. Once inside the bacterial cell, silver ions are known to interact with thiol groups of the proteins, whilst inactivating the enzymes (Liau, Read, Pugh, Furr, & Russell, 1997) and turning DNA into a condensed form, which may lead to damage or even death of the microorganisms (Feng et al., 2000; Kim et al., 2007).

Regarding the incubation time, the percentage of the surviving fraction of bacteria was higher after 3 h (Fig. 6, panels A and C) if compared to a longer incubation time (24 h, Fig. 6, panels B and D) for both bacterial strains ($p < 0.05$) even if it was more evident for *S. aureus* cells. Regarding the temperature of incubation, the percentage of viability for both bacterial strains was higher if incubated at 4 °C whereas it was markedly reduced at 24 °C and 37 °C (Fig. 6). These results are in agreement with the WAC data, thus confirming that the temperature influenced the diffusion and swelling properties of the PVA promoting a different diffusion path of Ag nanoparticles and release of Ag^+ ions. Moreover, at the temperature of 4 °C, the level of antibacterial activity for both bacterial strains was not influenced by the different kind of cellulose nanocrystals (CNC_MCC, CNC_ph or CNC_flax) or the different concentrations of Ag nanoparticles. At the temperatures of 24 °C and 37 °C, the percentage of bacteria viability was higher on PVA/CNC_MCC/Ag incubated with staphylococcal cells for 3 h and 24 h (Fig. 6, panels A and B) and *E. coli* cells for 3 h (Fig. 6, panel C) whereas was significantly decreased for *E. coli* cells at 24 h (Fig. 6, panel D) ($p < 0.05$). In contrast, at 24 °C and 37 °C the antibacterial activity was markedly greater on PVA/CNC_ph/Ag and further increased on PVA/CNC_flax/Ag films for *E. coli* at 3 h and 24 h (Fig. 6, panels C and D) and *S. aureus* at 24 h (Fig. 6, panel B) whereas it was reduced for *S. aureus* at 3 h (Fig. 6, panel A) ($p < 0.05$). In summary, for both strains, the antibacterial activity was stronger on PVA/1CNC_ph/0.5 Ag or PVA/1CNC_flax/0.5 Ag films containing 0.5 wt% of Ag nanoparticles if compared to PVA/1CNC_MCC/0.5% Ag when performed at 24 °C or 37 °C and at longer incubation times. In the first part of this work (Fortunati et al., 2013) we demonstrated that the presence of cellulose nanocrystals in PVA matrix leads to the variation on the intensity of —OH stretching, and this effect was more evident for CNC_MCC based systems. The revealed variation was attributed to the interaction between —OH group on the surface of CNC_MCC and the group —OH in the PVA matrix. This coupling effect can restrict the segmental mobility of the PVA chains (George et al., 2012), thus reducing the diffusion phenomena and consequently the Ag^+ release from the PVA/CNC_MCC based ternary systems limiting the antimicrobial response of these bio-nanocomposite formulation. In conclusion, the positive effect of CNC extracted from natural fibres (CNC_ph or CNC_flax) in supporting the active properties of PVA bionanocomposites, when compared to the CNC_MCC extracted from a commercial source, was demonstrated.

4. Conclusions

The study of ternary systems based on polyvinyl alcohol matrix, cellulose nanocrystals and silver nanoparticles, with CNC of different origin, (one commercial and two extracted from natural fibres) offered indications about their comparative potential for

applications in the packaging and biomedical sectors. With this aim, the structural, thermal, morphological and antibacterial properties of ternary systems, including two different contents of silver nanoparticles, 0.1 wt% and 0.5 wt%, were examined.

In general, CNC confer an effect of strengthening to the PVA matrix, to an extent comparable for all configurations, with the best values being offered by composites produced using flax fibres. This is confirmed also dealing with stiffness values, where a slight superiority is shown in contrast by composites including phormium fibres. However, the most significant effect on stiffness was revealed by the amount of Ag introduced, demonstrating that the ternary systems with 0.1 wt% of Ag were substantially superior for all configurations to those with 0.5 wt% of silver nanoparticles, though the latter might be preferable for a higher barrier effect to water absorption. On the 0.1 wt% silver nanoparticle based systems, also dynamic mechanical thermal analysis was performed, which yielded higher values of bulk modulus for the system with CNC from natural fibres.

On ternary systems, no significant modification in transition temperatures with respect to pure PVA films was measured by differential scanning calorimetry, so that both glass transition temperature and melting temperature did not show any significant change for any of the examined configurations. The same can be reported for thermal degradation patterns measured by thermogravimetry. It is also noteworthy that, in view of the envisaged applications, that systems including 0.1 wt% of Ag nanoparticles preserved their transparency properties with respect to pure PVA film.

The PVA bio-nanocomposite films showed an antibacterial activity against *S. aureus* and *E. coli* strains, which was more conclusive for the Gram negative strain. Furthermore, the antibacterial activity was dependent on the Ag content, the temperature of incubation and the type of cellulose nanocrystals used. In particular, activity was improved by using: (i) a higher content of Ag nanoparticles, (ii) a temperature of 24 °C or 37 °C and (iii) CNC extracted from natural phormium or flax fibres.

To sum up all the above considerations, this study suggests that on PVA/CNC/Ag ternary systems the effect of the origin of CNC is not negligible: in this particular case, systems with CNC from two natural fibres (flax and phormium) proved superior with those including CNC from commercial MCC. This is interesting, since in principle a number of ligno-cellulosic fibres are suitable for this purpose and are available in large quantities as by-products of other processes or agro-waste.

Acknowledgements

The authors gratefully acknowledge Prof. Juan López Martínez (Instituto de Tecnología de Materiales, Universitat Politècnica de València, Spain) and Dr. Marina P. Arrieta for TEM examinations.

References

Bin Ahmad, M., Lim, J. J., Shameli, K., Ibrahim, N. A., Tay, M. Y., & Chieng, B. W. (2012). Antibacterial activity of silver bionanocomposites synthesized by chemical reduction route. *Chemistry Central Journal*, http://dx.doi.org/10.1186/1752-153X-6-101

Bondeson, D., Mathew, A., & Oksman, K. (2006). Optimization of the isolation of nanocrystals from microcrystalline cellulose by acid hydrolysis. *Cellulose*, *13*, 171–180.

Bondeson, D., Syre, P., & Oksman, K. (2007). All cellulose nanocomposites produced by extrusion. *Journal of Biobased Materials and Bioenergy*, *1*, 367–371.

Chou, C. W., Hsu, S. H., Chang, H., Tseng, S. M., & Lin, H. R. (2006). Enhanced thermal and mechanical properties and biostability of polyurethane containing silver nanoparticles. *Polymer Degradation and Stability*, *91*, 1017–1024.

Cruthers, N. M., Carr, D. J., & Laing, R. M. (2006). Structural differences among fibers from six cultivars of harakeke (*Phormium tenax*, New Zealand flax). *Textile Research Journal*, *76*, 601–606.

De Rosa, I. M., Iannoni, A., Kenny, J. M., Puglia, D., Santulli, C., Sarasini, F., et al. (2011). Poly(lactic acid)/*phormium tenax* composites: Morphology and thermomechanical behaviour. *Polymer Composites*, *32*, 1362–1368.

Feng, Q. L., Wu, J., Chen, G. Q., Cui, F. Z., Kim, T. N., & Kim, J. P. (2000). A mechanistic study of the antibacterial effect of silver ions on *Escherichia coli* and *Staphylococcus aureus*. *Journal of Biomedial Materials Research*, *52*, 662–668.

Fischer, H., Werwein, E., & Graupner, N. (2012). Nettle fibre (*Urtica dioica* L.) reinforced poly(lactic acid): A first approach. *Journal of Composite Materials*, *46*, 3077–3087.

Fortunati, E., Armentano, I., Iannoni, A., & Kenny, J. M. (2010). Development and thermal behaviour of ternary PLA matrix composites. *Polymer Degradation and Stability*, *95*, 2200–2206.

Fortunati, E., Armentano, I., Zhou, Q., Iannoni, A., Saino, E., Visai, L., et al. (2012). Multifunctional bionanocomposite films of poly(lactic acid), cellulose nanocrystals and silver nanoparticles. *Carbohydrate Polymers*, *87*, 1596–1605.

Fortunati, E., Armentano, I., Zhou, Q., Puglia, D., Terenzi, A., Berglund, L. A., et al. (2012). Microstructure and nonisothermal cold crystallization of PLA composites based on silver nanoparticles and nanocrystalline cellulose. *Polymer Degradation and Stability*, *97*, 2027–2036.

Fortunati, E., Latterini, L., Rinaldi, S., Elisei, F., Kenny, J. M., & Armentano, I. (2011). PLGA/Ag nanocomposites: In-vitro degradation study and silver ion release. *Journal of Materials Science Materials in Medicine*, *22*, 2735–2744.

Fortunati, E., Puglia, D., Luzi, F., Santulli, C., Kenny, J. M., & Torre, L. (2013). Binary PVA bio-nanocomposites containing cellulose nanocrystals extracted from different natural sources: Part I. *Carbohydrate Polymers*, http://dx.doi.org/10.1016/j.carbpol.2013.03.075

Fortunati, E., Puglia, D., Monti, M., Santulli, C., & Kenny, J. M. (2012). Extraction of cellulose nanocrystals from *Phormium tenax* fibres. *Journal of Polymers and Environment*, http://dx.doi.org/10.1007/s10924-012-0543-1

Fortunati, E., Puglia, D., Monti, M., Santulli, C., Maniruzzaman, M., & Kenny, J. M. (2012). Cellulose nanocrystals extracted from okra fibres in PVA nanocomposites. *Journal of Applied Polymer Science*, http://dx.doi.org/10.1002/app.38524

Frone, A. N., Panaitescu, D. M., Donescu, D., Spataru, C. I., Radovici, C., Trusca, R., et al. (2011). Preparation and characterization of PVA composites with cellulose nanofibers obtained by ultrasonication. *BioResources*, *6*, 487–512.

Garkhail, S., Heijenrath, R., & Peijs, T. (2000). Mechanical properties of natural-fibre-mat-reinforced thermoplastics based on flax fibres and polypropylene. *Applied Composite Materials*, *7*, 351–372.

George, J., Vallayil, S. A., Ramana, K. V., Shanmugam, S. N., & Siddaramaiah. (2012). Augmented properties of PVA hybrid nanocomposites containing cellulose nanocrystals and silver nanoparticles. *Journal of Materials Chemistry*, *22*, 22433–22439.

Gautam, A., & Ram, S. (2010). Preparation and thermomechanical properties of Ag-PVA nanocomposite films. *Materials Chemistry and Physics*, *119*, 266–271.

Hassan, M. M., Mueller, M., Tartakowska, D. J., & Wagner, M. H. (2011). Mechanical performance of hybrid rice straw/sea weed polypropylene composites. *Journal of Applied Polymer Science*, *120*, 1843–1849.

Hepworth, D. G., & Bruce, D. M. (2000). The mechanical properties of a composite manufactured from non-fibrous vegetable tissue and PVA. *Composites: Part A*, *31*, 283–285.

Hughes, M. (2012). Defects in natural fibres: Their origin, characteristics and implications for natural fibre-reinforced composites. *Journal of Materials Science*, *47*, 599–609.

Kim, J. S., Kuk, E., Yu, K. N., Kim, J., Park, S. J., Lee, H. J., et al. (2007). Antimicrobial effects of silver nanoparticles. *Nanomedicine, Nanotechnology, Biology and Medicine*, *3*, 95–101.

Li, W. R., Xie, X. B., Shi, Q. S., Zeng, H. Y., Ou-Yang, Y. S., & Chen, Y. B. (2010). Antibacterial activity and mechanism of silver nanoparticles on *Escherichia coli*. *Applied Microbiology and Biotechnology*, *85*, 1115–1122.

Li, W., Yue, J., & Liu, S. (2012). Preparation of nanocrystalline cellulose via ultrasound and its reinforcement capability for poly(vinil alcohol) composites. *Ultrasonics Sonochemistry*, *19*, 479–485.

Liau, S. Y., Read, D. C., Pugh, W. J., Furr, J. R., & Russell, A. D. (1997). Interaction of silver-nitrate with readily identifiable groups – Relationship to the antibacterial action of silver ions. *Letters in Applied Microbiology*, *25*, 279–283.

Liu, D. Y., Yuan, X. W., Bhattacharyya, D., & Easteal, A. J. (2010). Characterisation of solution cast cellulose nanofibre-reinforced poly(lactic acid). *Express Polymer Letters*, *4*, 26–31.

Lok, C. N., Ho, C. M., Chen, R., He, Q. Y., Yu, W. Y., Sun, H., et al. (2007). Silver nanoparticles: Partial oxidation and antibacterial activitie. *Journal of Biological Inorganic Chemistry*, *12*, 527–534.

Mahanta, N., & Valiyaveettil, S. (2012). In situ preparation of silver nanoparticles on biocompatible methacrylated poly(vinyl alcohol) and cellulose based polymeric nanofibers. *RSC Advances*, *2*, 11389–21139.

Mbhele, Z. H., Salemane, M. G., Van Sittert, C. G. C. E., Nedeljkovic, J. M., Djokovic, V., & Luyt, A. S. (2003). Fabrication and characterization of silver–polyvinyl alcohol nanocomposites. *Chemistry of Materials*, *15*, 5019–5024.

Moran, J. I., Alvarez, V. A., & Cyras, V. P. (2008). Extraction of cellulose and preparation of nanocellulose from sisal fibers. *Cellulose*, *15*, 149–159.

Roohani, M., Habibi, Y., Belgacem, N. M., Ebrahim, G., Naghi Karimi, A., & Dufresne, A. (2008). Cellulose whiskers reinforced polyvinyl alcohol copolymers nanocomposites. *European Polymer Journal*, *44*, 2489–2498.

Sanchez-Garcia, M. D., Gimenez, E., & Lagaron, J. M. (2008). Morphology and barrier properties of solvent cast composites of thermoplastic biopolymers and purified cellulose fibers. *Carbohydrate Polymers*, *71*, 235–244.

Shanks, R. A., Hodzic, A., & Ridderhof, D. (2006). Composites of poly(lactic acid) with flax fibers modified by interstitial polymerization. *Journal of Applied Polymer Science*, *99*, 2305–2313.

Siqueira, G., Bras, J., & Dufresne, A. (2010). Cellulosic bionanocomposites: A review of preparation, properties and applications. *Polymers*, *2*, 728–765.

Taha, I. M., & Ziegmann, G. (2010). Potential of sisal reinforced biodegradable polylactic acid and polyvinyl alcohol composites. *Key Engineering Materials*, *425*, 167–178.

Vivekanandhan, S., Christensen, L., Misra, M., & Mohanty, A. K. (2012). Green process for impregnation of silver nanoparticles into microcrystalline cellulose and their antimicrobial bionanocomposite films. *Journal of Biomaterials and Nanobiotechnology*, *3*, 371–376.

Wang, Y., Tong, B., Hou, S., Li, M., & Shen, C. (2011). Transcrystallization behavior at the poly(lactic acid)/sisal fibre biocomposite interface. *Composites Part A: Applied Science and Manufacturing*, *42*, 66–74.

Wen-Ru, L., Xiao-Bao, X., Qing-Shan, S., Shun-Shan, D., You-Sheng, O., & Yi-Ben, C. (2011). Antibacterial effect of silver nanoparticles on *Staphylococcus aureus*. *Biometals*, *24*, 135–141.

Williams, R. L., Doherty, P. J., Vince, D. G., Grashoff, G. J., & Williams, D. F. (1989). The biocompatibility of silver. *Critical Reviews in Biocompatibility*, *5*, 221–243.